Journal of Hydrology 377 (2009) 112–119

Contents lists available at ScienceDirect

Journal of Hydrology

journal homepage: www.elsevier.com/locate/jhydrol

Colloid transport and remobilization in porous media during infiltration and drainage

Jie Zhuang [a,*], John S. Tyner [b], Edmund Perfect [c]

[a] Institute for a Secure and Sustainable Environment, Center for Environmental Biotechnology, Department of Biosystems Engineering and Soil Science, The University of Tennessee, Knoxville, TN 37996, United States
[b] Department of Biosystems Engineering and Soil Science, The University of Tennessee, Knoxville, TN 37996, United States
[c] Department of Earth and Planetary Sciences, The University of Tennessee, Knoxville, TN 37996, United States

ARTICLE INFO

Article history:
Received 6 November 2008
Received in revised form 11 June 2009
Accepted 7 August 2009

This manuscript was handled by P. Baveye, Editor-in-Chief

Keywords:
Colloid transport
Unsaturated flow
Transient flow
Flow rate
Ionic strength
Infiltration

SUMMARY

Colloids are potential vectors of many contaminants in porous media. Understanding colloid transport is critical for assessing the migration of contaminants (e.g., pathogens) in the vadose zone. In this study, a series of column experiments were conducted to investigate the coupled effects of flow velocity, water content, and solution ionic strength on transport and remobilization of a model colloid (montmorillonite clay) in a model porous medium (Accusand) during transient unsaturated flow and steady-state saturated flow. The unsaturated transport experiments included a series of infiltration and drainage pulses (e.g., infiltration with colloids, followed by drainage of colloid suspensions, followed by infiltration with a colloid-free solution and drainage of the solution). Saturated flow experiments included only the infiltration of the colloid and colloid-free solutions. Tests were repeated for a variety of solution ionic strengths. Results showed that colloid transport was more sensitive to changes in solution ionic strength at low infiltration rates, and the effect of infiltration rate was more significant at high ionic strength. As a result, increased flow velocities and water content, resulting from high infiltration rates, enhanced colloid transport and remobilization under ionic strength conditions (e.g., 100 mM) that would otherwise lead to strong colloid retention. This observation conceptually suggests that chemical threshold values for preventing colloid movement in porous media might be larger for transient flow conditions than for uniform flow conditions. In addition, drainage was found to induce remobilization of the retained colloids, suggesting transport of colloids even after termination of injection. Overall, the study experimentally highlights the complicated interdependence of the effects of water content, flow velocity, and solution chemistry on colloid transport and remobilization.

Introduction

Knowledge of colloid transport and mobilization in natural and engineered systems is of primary importance for the assessment and prediction of colloid-facilitated contaminant migration (McCarthy and Zachara, 1989; Grolimund et al., 1996; Zhuang et al., 2003). Over the past several decades, considerable advances have been made towards understanding the processes and corresponding mechanisms governing colloid deposition and transport through laboratory investigations, field studies, and numerical modeling (Kretzschmar et al., 1999; DeNovio et al., 2004; McCarthy and McKay, 2004). It has been recognized that colloid transport and mobilization is a function of many factors, including the properties of colloids and porous media (Bradford et al., 2002; Zhuang et al., 2004, 2005), solution chemistry (Elimelech and O'Melia, 1990a; Compere et al., 2001; Gamerdinger and Kaplan, 2001; Torkzaban et al., 2008), and flow conditions (Lenhart and Saiers, 2002; Saiers and Lenhart, 2003a; Zhuang et al., 2007; Shang et al., 2008). The dominant mechanisms controlling colloid transport and remobilization in porous media have been attributed to electrostatic, capillary, and shear forces (Ryan and Gschwend, 1994; Kretzschmar et al., 1997; Saiers and Lenhart, 2003a,b; Zhuang et al., 2004; Gao et al., 2006; Shang et al., 2008). Electrostatic forces are an important component of the total interaction energy between colloids and the porous medium and are impacted by factors influencing the electric double layer (EDL), such as solution ionic strength, ion composition, and pH. Capillary forces describe interactions between individual colloids or between colloids and surfaces wetted by fluid and are impacted by the degree of saturation, pore sizes, contact angles of both colloids and porous media, and surface tension (Kralchevsky et al., 1992; Kralchevsky and Nagayama, 2000; Kralchevsky and Denkov, 2001). Shear force is the shear developed on the wetted area of the pore channel. It acts

* Corresponding author. Tel.: +1 865 974 1325; fax: +1 865 974 1838.
E-mail address: jzhuang@utk.edu (J. Zhuang).

0022-1694/$ - see front matter © 2009 Elsevier B.V. All rights reserved.
doi:10.1016/j.jhydrol.2009.08.011

in the direction of flow and is impacted by the flow velocity, liquid density, and flow path tortuosity (Simons and Sentürk, 1992). Most previous colloid transport studies included only steady-state flow conditions, which do not effectively represent natural vadose zones, where transient flows (e.g., infiltration and drainage) tend to dominate.

More recently, several studies have addressed transient transport of colloids by studying the influence of physical and chemical perturbations on colloid transport and mobilization. For example, Saiers and Lenhart (2003a) and Shang et al. (2008) reported that a stepwise increase in the flow rate during unsaturated flow can substantially increase colloid movement. A number of studies (Crist et al., 2004, 2005; Zevi et al., 2005; Lazouskaya et al., 2006) visualized the redistribution of colloids during drainage of pore water. They found that colloids responded to changes in the distribution, configuration, and total area of air–water menisci. During the drainage process, colloids accumulate in the thin water films present at air–water–solid contacts. Although there are alternative arguments in the literature describing how air–water interfaces and/or air–water–solid interfaces affect colloid retention and mobilization (Wan and Tokunaga, 2005; Steenhuis et al., 2005), it seems that changes in pore water saturation and the geometry of corner-water ducts in porous media can cause colloid remobilization (Gao et al., 2006).

The transient transport of colloids may also be subject to the coupling of flow and chemical conditions. This is because, under certain conditions, capillary and shear forces create separation distances between colloids and pore walls beyond which the electric double layer (EDL) is ineffective in influencing the electrostatic component of the total interaction energies, thus reducing the importance of solution chemistry on colloid retention. To our knowledge, the combined effect of transient unsaturated flow (e.g., infiltration and drainage cycles) and solution chemistry (e.g., ionic strength) on the transport of colloids remains unexamined. A systematic study of the interactions between these factors is thus essential for understanding colloid transport in the vadose zone. The objective of this study was to examine the coupled effects of infiltration rate, water content, and solution ionic strength on the transport and remobilization of colloids during transient unsaturated flow within a porous medium as compared to steady-state saturated flow. Drainage-induced colloid mobilization was also addressed.

Materials and methods

Porous medium and colloid properties

Silica sand (Accusand, grade 20/30, Unimin Corporation, Le Sueur, MN) was used as the model porous medium in the transport experiments. The sand grains had a median diameter (d_{50}) of 0.71 ± 0.02 mm and a cation exchange capacity of 0.57 cmol/kg according to specifications provided by Unimin Corporation. The total carbon content in the original sand was measured to be 0.3 g/kg using a Shimadzu TOC-V organic carbon analyzer with a solid sample module. The saturated hydraulic conductivity was determined to be 784 ± 11 cm/h using the constant-head method (Klute and Dirksen, 1986). The drainage water retention curve was measured with a Tempe pressure cell (Soil Moisture Equipment Inc., Model 1400B1M2-3) (Dane and Hopmans, 2002), and parameterized by fitting the van Genuchten equation (Van Genuchten, 1980) using non-linear regression, yielding $S_e = [1 + (0.0744\psi)^{8.47}]^{-0.882}$, where ψ is the absolute value of soil matric potential (cm), and $S_e = (\theta - \theta_r)/(\theta_s - \theta_r)$ with θ the volumetric water content (m^3/m^3) and the subscripts s and r denoting the saturated and residual water contents, respectively. The value of θ_s was assumed to be equal to the total porosity of the packed sand (~0.33% m^3/m^3), and the value of θ_r was obtained by measuring the water content of the air-dried sand (~0.027% m^3/m^3). Prior to packing the columns, the sand was thoroughly rinsed with particle-free deionized water (5.5×10^{-7} dS/cm) to remove any suspended impurities and was then oven-dried at 60 °C.

Montmorillonite, a 2:1 clay that occurs widely in natural soils, was selected for the model colloid. The original Na-rich montmorillonite powder (SWy-2, Crook County, Wyoming) was purchased from the Source Clays Repository at the University of Missouri. To obtain particles smaller than 1-μm in diameter, the powder was first dispersed in deionized water using a probe ultrasonicator at 10 J/s for 10 min, and the <1-μm particles were then extracted from the suspension by gravity settling using a 1000-mL graduated cylinder (Gee and Or, 2002). After being concentrated in a polypropylene beaker at 60 °C, the extracted montmorillonite slurry was refrigerated at 6 °C for subsequent preparation of the colloid input solutions. The montmorillonite particles aggregated and their surface potentials changed with solution ionic strength. We therefore measured their effective particle diameters and zeta potentials in all the experimental solutions (2–100 mM $NaNO_3$) with a ZetaPals analyzer (Brookhaven Instrument Ltd.) (Table 1).

Column experiments

One-dimensional vertical column experiments were conducted under transient unsaturated and steady-state saturated flow conditions. A summary of the experimental initial and boundary conditions for the different tests is provided in Table 2. The different infiltration rates created a broad range of pore water saturations. To facilitate comparison with different-textured porous media from other studies, the infiltration rate is expressed as a percentage of the sand saturated hydraulic conductivity (K_s) (Zhuang et al., 2007). The range of selected solution ionic strengths (Table 2) considered both natural salt levels in the vadose zone and the possibility of chemical spills.

The testing apparatus employed during the unsaturated and saturated experiments is illustrated in Fig. 1. All water was applied to the upper boundary for the unsaturated experiments and to the lower boundary for the saturated experiments. Time series effluent samples were collected from all experiments with a fraction collector. For the unsaturated experiments, a 5.5 kPa tension was applied to the bottom boundary by placing a 20-μm nylon membrane with a 6.4 kPa air-entry value (Spectra/Mesh, Spectrum Laboratories, Inc.) on the base of the column and attaching the membrane to a vacuum system, which included a vacuum chamber (CL-040, Soil Measurement Systems, Tucson, AZ) and vacuum control valves (Type 70, Bellofram Corp., Newell, WV).

The column was made of clear Schedule-40 PVC pipe, with 2-cm inner diameter and 60-cm height. Two aeration holes (2-mm in diameter) were drilled at two depths (23.5 cm and 58.5 cm) on opposite sides of the column wall to evacuate air during infiltration. The holes were temporarily sealed with parafilm for the initial flushing and saturated flow experiments. Teflon tubing was used throughout the system except for a short section of tygon tubing used in the peristaltic pump.

To prepare for the column experiments, we filled the empty columns to a height of ~5 cm with deaired colloid-free $NaNO_3$ back-

Table 1
Colloid size and zeta potential in $NaNO_3$ solutions.

Ionic strength (mM)	Effective diameter (nm)	Zeta potential (mV)
2	512 ± 8	−40.3 ± 0.8
20	709 ± 13	−31.3 ± 4.1
100	1573 ± 75	−24.6 ± 1.0

Table 2
Column experimental conditions.

Exp. #.	Flow condition	Infiltration rate		Ionic strength (mM)	Initial water content (m^3/m^3)	Bulk density (Mg/m^3)	Porosity[a]
		mm/h	(% K_s)				
1	Unsaturated	52	0.7	2	0.029	1.82	0.33
2	Unsaturated	52	0.7	20	0.035	1.81	0.33
3	Unsaturated	52	0.7	100	0.034	1.82	0.33
4	Unsaturated	516	6.6	2	0.031	1.82	0.33
5	Unsaturated	516	6.6	20	0.034	1.82	0.33
6	Unsaturated	516	6.6	100	0.034	1.81	0.33
7	Unsaturated	1031	13.2	2	0.033	1.78	0.34
8	Unsaturated	1031	13.2	20	0.032	1.81	0.33
9	Unsaturated	1031	13.2	100	0.036	1.82	0.33
10	Saturated	52	0.7	2	0.322	1.83	0.32
11	Saturated	52	0.7	100	0.319	1.84	0.32
12	Saturated	1031	13.2	2	0.329	1.81	0.33
13	Saturated	1031	13.2	100	0.326	1.82	0.33

[a] Estimated from bulk density using a particle density of 2.7 g/cm^3.

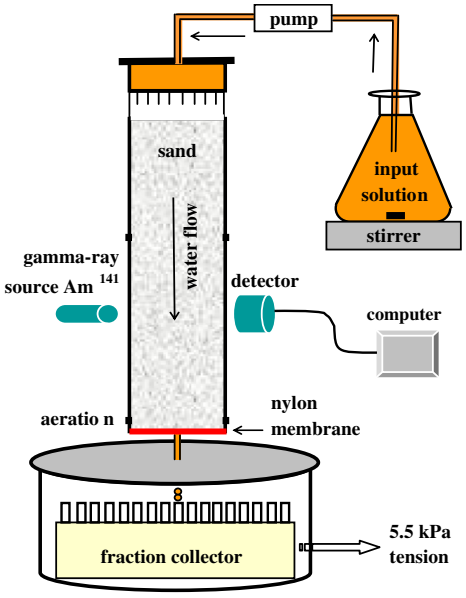

Fig. 1. Schematic of the unsaturated column system used in the study.

ground solution (2–100 mM, pH 6.7). Dry sand was then slowly poured into the solution in 1-cm increments while being stirred and gently tapped to avoid air entrapment and to ensure uniform packing. To remove any *in situ* colloids present in the rinsed sand and to allow a chemical equilibration of the sand pack with the background solution, the packed columns were flushed with ~5 pore volumes of deaired $NaNO_3$ solution prior to each experiment. Following flushing with a peristaltic pump, each column was drained overnight with a constant lower boundary tension (5.5 kPa) and the top covered by a sparsely punctured parafilm. After the drainage, the average water saturation was determined gravimetrically to be 10.6 ± 1.5% (i.e., 0.035 ± 0.005 m^3/m^3).

Each infiltration experiment was initiated by pumping the input solution upward from the bottom of the column (saturated experiments) or by dripping it onto the upper sand surface via a sprinkler system (unsaturated experiments) at a constant injection rate and at room temperature (22 ± 1 °C). The sprinkler system was attached to a peristaltic pump and consisted of an injection chamber (1.9-cm i.d. and 3-cm height) with seven 26-gauge hypodermic needles arranged uniformly across the bottom of the chamber (Fig. 1). The input solution included a range of $NaNO_3$ concentrations (2–100 mM) along with 250 mg/L montmorillonite colloids. The influent colloid concentration was selected by considering the minimum detection limit of analysis of the effluent colloid concentrations. The unsaturated flow experiments sequentially included four stages: colloid injection, overnight drainage, elution with colloid-free solution, and a second overnight drainage. The lower boundary tension (5.5 kPa) was maintained throughout all four stages of the transient unsaturated flow experiments. During the colloid injection stage, ~90 mL of the colloid suspension was introduced into the column before the first overnight drainage. The following day another elution with ~90 mL of colloid-free $NaNO_3$ solution (the same ionic strength) was applied. After the effluent colloid concentration returned to the baseline level (about 0.1–0.5 mg/L mineral particles as estimated during pre-flush by UV–Vis spectrophotometer at a wavelength of 350 nm) the injection at the top of the column was halted to allow the second overnight drainage. Throughout the experiment, the influent reservoir was slowly stirred, and the effluent was collected in 10-mL glass test tubes at regular time intervals (0.3, 1, and 10 min for infiltration rates of 13.2% K_s, 6.6% K_s, and 0.7% K_s, respectively). A test with blue food dye (McCormick & Company, Inc.) that was mixed with pre-flush solution indicated that preferential flow did not occur when water infiltrated into the preflushed wet sand. Six of the nine experiments were replicated, and the colloid breakthrough curves were very consistent with each other (one-way analysis of covariance $P > 0.2$). The saturated transport experiments consisted of colloid injection and elution under steady-state flow conditions (no drainage involved). Final montmorillonite concentrations in the effluent were determined by measuring the aluminum concentration of each sample with an ICP-MS (IRIS Intrepid II XSP, Thermo Electron Co.) operating at a wavelength of 308.96 nm. Prior to the colloid analysis, all effluent samples were sonicated for 1 min.

In Situ water content measurement using gamma-ray attenuation system

A custom-built gamma-ray attenuation system (Fig. 1) monitored the spatial and temporal changes of volumetric water content during the infiltration and drainage stages of the unsaturated experiments. Water contents were measured at four depths (25, 35, 45 and 57 cm), which were based on optimizing the maximum number of monitored locations while minimizing the travel time of the gamma-ray attenuation system between monitoring locations. The system was programmed to scan the selected depths throughout the infiltration and drainage stages using a data acquisition system and software-controlled linear actuator

(Bislide 15 in., MN-0150-E01–21) and stepping motor. Further details about the system are provided in Tyner and Brown (2004).

Prior to infiltration, the preflushed-then-drained columns were scanned vertically to determine the gamma-ray attenuation caused by the sand and initial water content. The counting live-time was 10 s at each depth, which resulted in a measurement deviation of <10% compared to the actual volumetric water content. The duration of one complete column scan was about 3 min including the travel time of the detector between the four depths. Spatial and temporal changes in water content during the flow experiments were calculated based on the attenuation of gamma-radiation by water using the Lambert–Beer equation (Oostrom et al., 2002) and the known mass attenuation coefficient of water, μ_w. The experimentally determined value of μ_w agreed well with the theoretical value, indicating that the system was well collimated.

Results and discussion

Water infiltration and drainage at different infiltration rates

Fig. 2 shows the changes in water saturation during infiltration and drainage of the sand. Only, data obtained from experiments using the 2 mM $NaNO_3$ solution are representatively shown because similar results were observed at 20 mM and 100 mM. In all cases, the water saturation increased very quickly during the initial infiltration, and then stabilized at a high level through the infiltration stage, followed by a decrease during drainage. The stable water saturation during the infiltration period suggests that a steady-state flow condition was maintained throughout the column during the period between the initial outflow and the beginning of drainage. The steady-state water saturations (0.30, 0.38, and 0.47) increased with increasing infiltration rate (i.e., 0.7% K_s, 6.6% K_s, and 13.2% K_s, respectively). The travel times for the wetting fronts to reach the bottom of the column were 38, 7, and 5 min for the infiltration rates of 0.7% K_s, 6.6% K_s, and 13.2% K_s, respectively. By observing the elapsed time between the end of imbibition and the return of the antecedent saturation at the column base (57 cm depth), we observed that the desaturation front required 4, 12, and 16 min to reach the bottom of the columns at infiltration rates of 0.7% K_s, 6.6% K_s, and 13.2% K_s, respectively. These varying infiltration and drainage rates, and associated changes in water contents, were expected to influence colloid transport and mobilization.

Effect of ionic strength on colloid transport and remobilization

Transient infiltration, drainage, and elution of montmorillonite colloids through the silica sand at three ionic strengths (2, 20, and 100 mM $NaNO_3$) and three infiltration rates (0.7% K_s, 6.6% K_s, and 13.2% K_s) are compared in Fig. 3. During the colloid injection stages (Fig. 3a, c and e), the colloid concentrations showed a rising trend in the initial effluent, and then climbed up to a relatively stable level after an outflow of ~10-mL. The relative change of colloid concentration approximated the change in saturation (an initial rapid increase followed by a stable value). This pattern is similar to the colloid breakthrough curves observed in studies conducted with partially saturated porous media under steady-state flow conditions (Lenhart and Saiers, 2002; Zhuang et al., 2005). Under steady-state flow conditions, the relatively low colloid breakthrough concentrations at early times were attributed primarily to colloid dispersion, attachment at solid–water interfaces, and straining by water films or pore throats (Elimelech and O'Melia, 1990a; Wan and Tokunaga, 1997; Bradford et al., 2002; Zevi et al., 2005; Zhuang et al., 2005; Gao et al., 2006). However, when subjected to transient flow conditions, these dynamic colloid concentrations appear

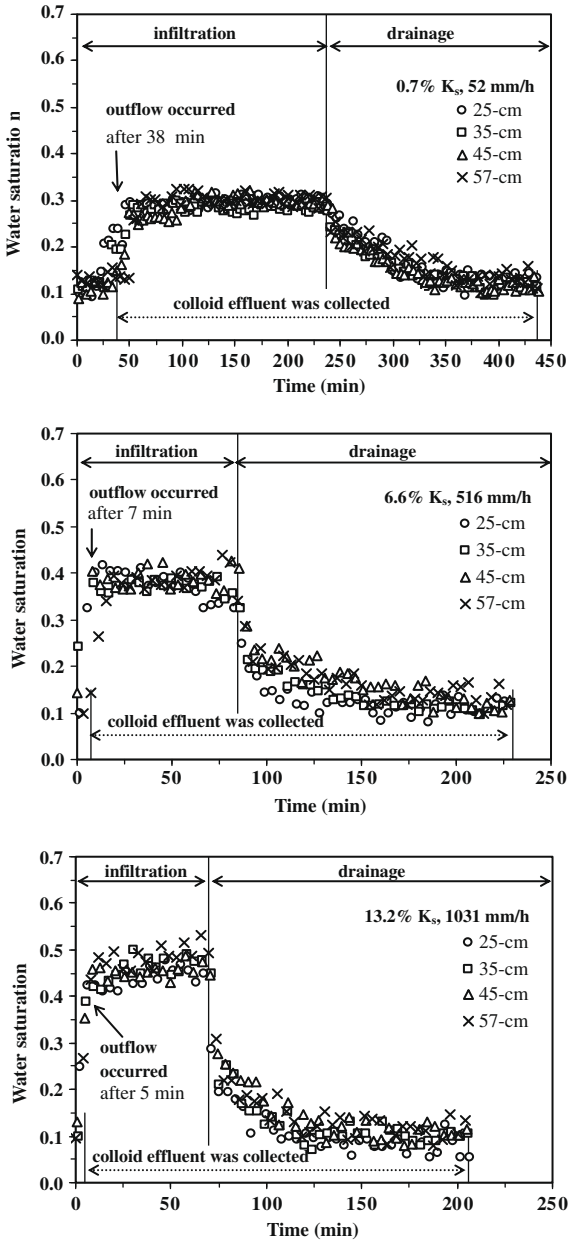

Fig. 2. Temporal changes in water saturation at different depths of the column during infiltration and drainage of 2 mM $NaNO_3$ solution.

to be dominated by changes in water content, as noted above. Air–water interfaces were assumed not to play a significant role. Wan and Tokunaga (2002) found that Na-montmorillonite clays were excluded from air–water interfaces (at any pH and ionic strength) due to the high electro-negativity of the particles. However, Crist et al. (2004, 2005) reported that colloids could also be retained at the air–water–grain interface and are thus subjected to the change in pore water saturation and geometry.

The difference in effluent colloid concentration observed for both the initial transient portion of the pulse and the later steady-state flows (i.e., the plateau portion of the curves in Fig. 3a, c and e) among the different ionic strengths indicates a pronounced electrostatic effect. The lower ionic strengths favored colloid transport at the lowest infiltration rate (0.7% K_s). The stable colloid concentrations (C/C_0) reached ~0.89 and ~0.60 for 2 mM and 20 mM solutions, respectively, in contrast to the very low level (only ~0.05–0.1) for 100 mM solution (Fig. 3a). This io-

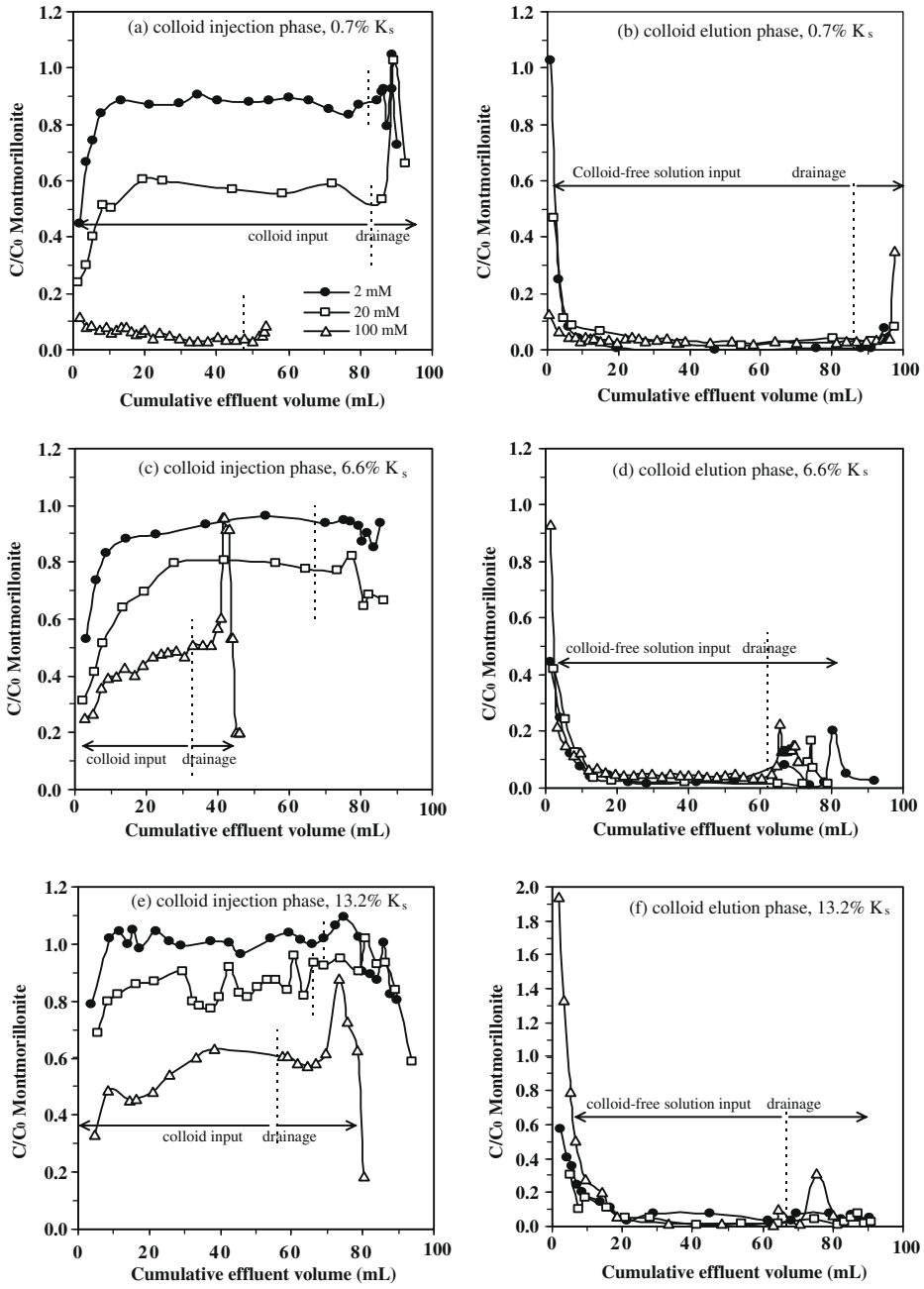

Fig. 3. Effects of infiltration rate and ionic strength on the transport and remobilization of montmorillonite in silica sand during infiltration and drainage. The elution was performed using colloid-free solutions with the same ionic strength and pH as used in the colloid injection phases. The vertical dashed lines indicate liquid input stage to the left of the lines and drainage stage to the right of the lines. Note the scale of *y*-axis in (f) is different from others.

nic strength effect was further verified by the saturated transport results. Fig. 4 shows that for steady-state saturated flow the stable C/C_0 was 0.95 for the 2 mM solution, but only 0.08 for the 100 mM solution at 0.7% K_s. These values are consistent with theoretical calculations on the electrostatic interaction energies for the three ionic strengths (data not presented) and previous studies (e.g., Tien and Payatakes, 1979; O'Melia, 1990; Elimelech and O'Melia, 1990a; Compere et al., 2001; Gamerdinger and Kaplan, 2001; Saiers and Lenhart, 2003b). In addition to the increased electrostatic interaction energies between colloids and sand grains, the greater retention of colloids at 100 mM can also be attributed to the formation of larger aggregates (Table 1). The increase in effective colloid diameter would increase retention through straining, filtration, and/or enhanced collection efficiency via aggregate settling (Song and Elimelech, 1993; Bradford et al., 2002, 2003; Saiers and Lenhart, 2003a).

The column elution characterized the detachment or remobilization of the colloids retained within the sand during the colloid injection stages (Fig. 3b, d and f). In the steady-state saturated flow experiments, the steep decrease of colloid concentration during the elution stage (i.e., the descending limbs of the curves in Fig. 4) indicates that detachment of the colloids retained at water–solid interfaces was minimal. However, during the transient unsaturated flow experiments the colloid concentration peaked coincidently with the initial breakthrough of the injected colloid-free solution, followed by a rapid decline of C/C_0 to a constant low concentration after ~10-mL of cumulative outflow. This trend agrees well with the descriptions of *in situ* colloid mobilization during infiltration

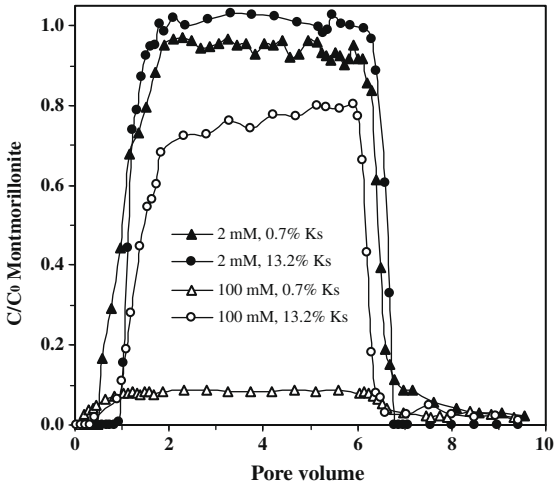

Fig. 4. Effects of ionic strength and infiltration rate on montmorillonite transport through the silica sand under saturated steady-state flow conditions.

or rainfall events (Kaplan et al., 1993; Worrall et al., 1999; El-Farhan et al., 2000; Zhuang et al., 2007). Likely processes include colloid release to fluid streamlines and mobilization by hydrodynamic shear. As the wetting front of the colloid-free solution moved into less water-saturated sand, colloids that were trapped in disconnected areas of pendular water or strained at air–water–grain interfaces were likely released and mobilized as the saturation increased (Kaplan et al., 1993; Gao et al., 2006; Zhuang et al., 2007). As a result, the first column outflow was characterized by a peak in colloid concentration and mass. Variation of the peak colloid concentrations with ionic strength and infiltration rate during elution (Fig. 3b, d and f) was most likely related to the amount and mobility of colloids (e.g., due to the colloid size effect) that were retained within the sand matrix during the colloid injection stages. The large colloid concentrations observed during the elution with 100 mM $NaNO_3$ at the two higher infiltration rates (i.e., 6.6% and 13.2% K_s) (Fig. 3d and f) probably resulted from the larger resident colloid concentrations and greater changes in saturation and associated extension/shrinkage of air–water and/or air–water–grain interfaces. Recovery calculations show that 2.04, 5.84, and 6.29 mg montmorillonite were retained within the sand columns prior to the elution at an infiltration rate of 6.6% K_s (Fig. 3d) in the 2, 20, and 100 mM ionic strength solutions, respectively. Correspondingly, 0.11, 3.56, and 8.79 mg colloids were retained before the elution at 13.2% K_s (Fig. 3f) for 2, 20, and 100 mM, respectively. In contrast, a negative relationship ($y = -0.09x + 1.33$, $R^2 = 0.99$, $n = 3$) existed between the resident colloid mass (x, mg) and the magnitude of the colloid elution peaks (y, C/C_0) at the lowest infiltration rate (0.7% K_s). Such a relationship might be due to the limited effect of the small change in pore water configuration on colloid mobilization at the low infiltration rate. However, these speculations are based only on colloid breakthrough results and verification at the pore scale is necessary.

Effect of infiltration rate on colloid transport and remobilization

Fig. 3a, c and e demonstrate that the effluent colloid concentrations in the colloid injection stages increased with increasing infiltration rate at each ionic strength. A unit increase in % K_s increased both the initial and the maximum stable colloid concentration by ~0.02–0.04 regardless of the ionic strength. This relationship, however, does not apply to the colloid remobilization that occurred during the column elution stage. Peak colloid concentration increased by ~0.14 per unit increase in % K_s at 100 mM, but there was no consistent trend at 2 mM or 20 mM. This apparent infiltration rate effect was due to the coupled effects of flow velocity and water content, which concurrently increased with increasing infiltration rate (Fig. 2). Several column-scale studies (Kretzschmar et al., 1997; Compere et al., 2001; Zhuang et al., 2004) suggest that larger flow velocities permit more colloids to remain in streamlines by decreasing the thickness of the shear interface between the mobile and immobile water phases. Other studies (Wan and Tokunaga, 1997; Lenhart and Saiers, 2002; Saiers and Lenhart, 2003b; Gao et al., 2006) maintain that an increase in water content reduces mechanical and film straining of colloids in unsaturated sand by expanding flow pathways (water films and corner-water ducts) and enhancing pore water continuity.

Interaction between ionic strength and infiltration rate effects

The interaction between ionic strength and infiltration rate was observed during both saturated and unsaturated flow. The steady-state saturated transport experiments (Fig. 4) show that a unit increase in % K_s increased C/C_0 by 0.006 and 0.053 at 2 mM and 100 mM, respectively, suggesting a larger infiltration rate effect at higher ionic strength (increased by a factor of about nine). Conversely, the ionic strength effect was smaller at higher infiltration rates. A unit decrease in ionic strength (mM) increased C/C_0 by 0.003 at 13.2% K_s and 0.009 at 0.7% K_s.

To summarize the unsaturated experimental results (Fig. 3), we plotted the maximum stable effluent colloid concentrations observed in the colloid injection phases and the cumulative percentage of colloids recovered in the effluent as a function of solution ionic strength and infiltration rate in Fig. 5a and b. Colloid mobility increased with increasing infiltration rate and decreasing ionic strength. The slopes decreased as the infiltration rate increased from 0.7% K_s to 6.6% K_s suggesting that the ionic strength effect decreased with increasing water content and flow velocity. The similarity of the colloid concentration slopes and percent mass recovery curves between the infiltration rates of 6.6–13.2% K_s was likely due to exceeding the threshold values for water content and flow velocity beyond which the ionic strength effect is minimal. The greater differences in maximum stable C/C_0 and mass recovery at 100 mM than at 2 mM and 20 mM indicate that the coupled effects of water content and flow velocity increased with increasing ionic strength. Multiple regression analysis of the data presented in Fig. 5a and b showed that the maximum stable C/C_0 or colloid recovery mass was linearly correlated to the infiltration rate and the ionic strength (Fig. 5c and d). Near matches of the estimated and measured values (i.e., the data lie close to a 1:1 line) indicate that the regression equations accurately predicted the impacts of infiltration rate and ionic strength.

The coupling of the infiltration rate effect and the ionic strength effect was presumably due to the difference of effective colloid size under different flow conditions. Colloid size has been documented to be one of the most important factors that influence colloid transport and deposition (Ruckenstein and Prieve, 1976; Elimelech and O'Melia, 1990b; Litton and Olson, 1996; Huber et al., 2000; Zhuang et al., 2005). Table 1 shows that colloids aggregated at high ionic strength, and that the effective aggregate sizes (y, nm) were linearly correlated to the ionic strength (x, mM): $y = 10.8x + 491.4$ ($R^2 = 1.00$, $n = 3$). Such an increase in aggregate size could (1) reduce colloid dispersion due to a decrease in colloid-sand collisions, (2) increase mechanical straining due to clogging in pore channels and down-gradient throats (Bradford et al., 2002, 2003), and (3) make colloid movement more sensitive to any change in drag/shear force (Ko et al., 2000; Zhuang et al., 2004). This interaction of aggregated colloid size with flow-velocity/water-content and solution ionic strength partly explains the apparently increased ef-

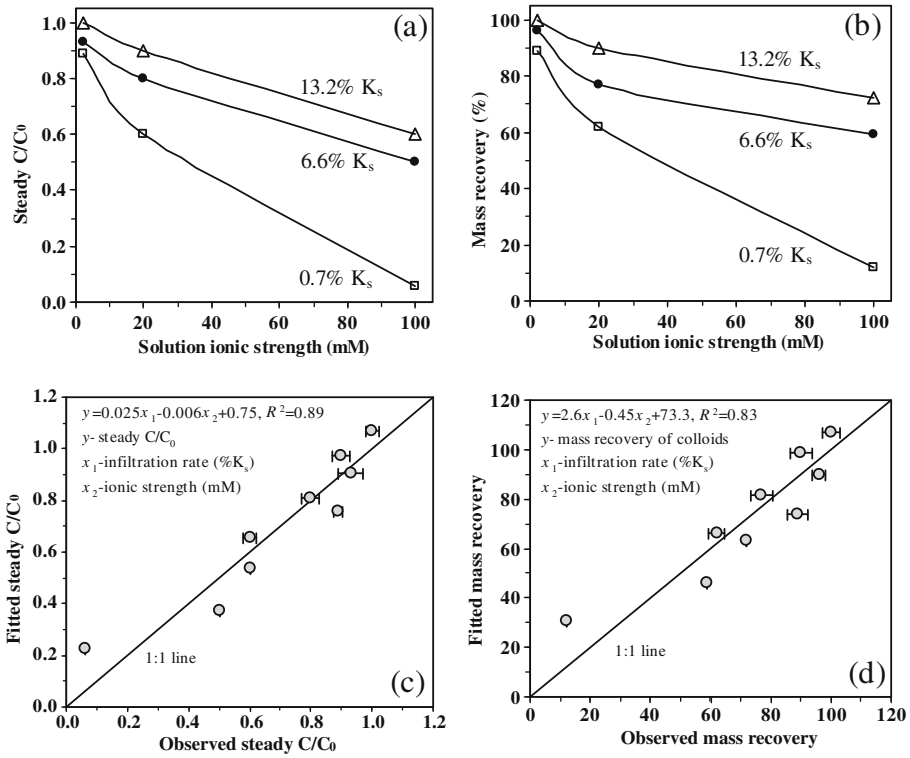

Fig. 5. Coupled effects of infiltration rate and ionic strength on the transport of montmorillonite through the silica sand during infiltration and drainage. The transport is quantified in terms of (a) normalized steady concentration (C/C_0) of montmorillonite in the effluent and (b) mass recovery of montmorillonite, which was calculated as the percentage of montmorillonite collected during the injection phase and the elution phase relative to the total mass of the introduced montmorillonite. Error bars are only available for the six repeated unsaturated experiments.

fect of infiltration rate on colloid movement as ionic strength increased.

Drainage-induced colloid remobilization

For all the ionic strengths, water drainage began with an outflow rate of ~0.23, ~2.4, and ~5.0 mL/min for the 0.7% K_s, 6.6% K_s, and 13.2% K_s experiments, respectively. A colloid release peak occurred as the water saturation decreased during the drainage that followed the colloid injection and column elution (Fig. 3). Although the magnitudes of the peaks were small and inconsistent among the different experiments, the peaks were more obvious at higher ionic strength (e.g., 100 mM). This drainage-induced pulse of colloid release was also reported by Saiers et al. (2003), who found that the effluent colloid concentrations increased during drainage and peaked in the last sample that marked the arrival of the desaturation front at the bottom of the column. Zhuang et al. (2007) also demonstrated a surging elution peak of *in situ* colloids from Hanford sediments near the end of the drainage process.

Similar to the mechanisms responsible for colloid transport during infiltration, the drainage effect is a result of the coupled effects of flow velocity, water content, and ionic strength. During drainage, the desaturation front moves downwards. Behind the front, the pore water saturation decreases, water menisci shrink, and air–water/air–water–grain interfaces increase in area. According to the literature (Kralchevsky et al., 1992; Kralchevsky and Nagayama, 2000; Saiers et al., 2003; Crist et al., 2004, 2005; Gao et al., 2006), all of these changes can lead to colloid mobilization. As a result, the desaturation front apparently scoured the colloids that were trapped in the sand causing an abrupt increase in effluent colloid concentration as the desaturation front exited the column. The small peaks occurring during drainage in the 2 mM $NaNO_3$ solution at all infiltration rates were probably related to the small amount of colloids retained in the column. The much larger colloid release peaks at the two higher infiltration rates (i.e., 6.6% K_s and 13.2% K_s) with 100 mM $NaNO_3$ (Fig. 3c and e) are speculated to result from the larger drainage flux. Pore-scale investigations will be necessary for verification of the underlying mechanisms.

Concluding remarks

This study demonstrates the coupling of flow velocity, water content, and ionic strength effects on colloid transport and mobilization during transient unsaturated flow as compared to steady-state saturated flow. An increase in infiltration rate, which caused a concurrent increase in flow velocity and pore water saturation, promoted colloid transport through the porous medium. The infiltration rate effect became larger with increasing solution ionic strength, which increased both the colloid-sand electrostatic interactions and the colloid aggregate size. The experiments also revealed a secondary peak of colloid release during water drainage. These secondary peaks were linearly correlated to solution ionic strength and infiltration rate. The mechanism responsible for the secondary peaks is inferred to be the transferal of trapped colloids with moving water menisci from regions of low to high water saturation as the desaturation front moves. This study suggests that the coupled effects of flow velocity, water content, and ionic strength must be examined concurrently to describe colloid transport in the vadose zone. Unfortunately, the relative magnitudes of capillary and shear forces could not be determined because of the uncertainties in the frequency and extent of colloid collision with the sand under transient flow conditions, and an inability to quantify flow velocities during infiltration and drainage. Nevertheless, our results provide novel and significant insights into the interactions among electrostatic, capillary, and shear forces when colloids are transported under transient unsaturated flow conditions. Such conditions often prevail in unsaturated porous media during storm

events, snow-melt, and septic fields when water is discharged, making our findings highly relevant to the facilitated transport of pathogens as well as toxic metal and organic contaminants with an affinity for adsorbing to colloidal particles.

Acknowledgements

The study was supported by the Environmental Management Science Program, US Department of Energy under Grant No. DE-FG07-02ER63496. We thank Dr. John F. McCarthy and Dr. Markus Flury for their review and editing of an early version of the manuscript. We also thank Dr. Tammo Steenhuis and an anonymous reviewer for their very helpful and insightful comments.

References

Bradford, S.A., Yates, S.R., Bettahar, M., Simunek, J., 2002. Physical factors affecting the transport and fate of colloids in saturated porous media. Water Resour. Res. 38, 1327. doi:10.1029/2002WR001340.

Bradford, S.A., Simunek, J., Bettahar, M., van Genuchten, M.Th., Yates, S.R., 2003. Modeling colloid attachment, straining, and exclusion in saturated porous media. Environ. Sci. Technol. 37, 2242–2250.

Compere, F., Porel, G., Delay, F., 2001. Transport and retention of clay particles in saturated porous media: influence of ionic strength and pore velocity. J. Contam. Hydrol. 49, 1–21.

Crist, J.T., McCarthy, J.F., Zevi, Y., Baveye, P., Throop, J.A., Steenhuis, T.S., 2004. Pore-scale visualization of colloid transport and retention in partly saturated porous media. Vadose Zone J. 3, 444–450.

Crist, J.T., Zevi, Y., McCarthy, J.F., Throop, J.A., Steenhuis, T.S., 2005. Transport and retention mechanisms of colloids in partially saturated porous media. Vadose Zone J. 4, 184–195.

Dane, J.H., Hopmans, J.M., 2002. Pressure cell. In: Dane, J.H., Topp, G.C. (Eds.), Methods of Soil Analysis, Part 4-Physical Methods. ASA and SSSA, Madison, WI, pp. 684–688.

DeNovio, N.M., Saiers, J.M., Ryan, J.N., 2004. Colloid movement in unsaturated porous media: recent advances and future directions. Vadose Zone J. 3, 338–351.

El-Farhan, Y.H., Denovio, N.M., Herman, J.S., Hornberger, G.M., 2000. Mobilization and transport of soil particles during infiltration experiments in an agricultural field, Shenandoah Valley, Virginia. Environ. Sci. Technol. 34, 3555–3559.

Elimelech, M., O'Melia, C.R., 1990a. Kinetics of deposition of colloidal particles in porous media. Environ. Sci. Technol. 24, 1528–1536.

Elimelech, M., O'Melia, C.R., 1990b. Effect of particle-size on collision efficiency in the deposition of Brownian particles with electrostatic energy barriers. Langmuir 6, 1153–1163.

Gamerdinger, A.P., Kaplan, D.I., 2001. Colloid transport and deposition in water-saturated Yucca Mountain tuff as determined by ionic strength. Environ. Sci. Technol. 35, 3326–3331.

Gao, B., Saiers, J.E., Ryan, J.N., 2006. Pore-scale mechanisms of colloid deposition and mobilization during steady and transient flow through unsaturated granular media. Water Resour. Res. 42, W01410. doi:10.1029/2005WR004233.

Gee, G.W., Or, D., 2002. Particle-size analysis. In: Dane, J.H., Topp, G.C. (Eds.), Methods of Soil Analysis, Part 4-Physical Methods. ASA and SSSA, Madison, WI, pp. 269–278.

Grolimund, D., Borkovec, M., Barmettler, K., Sticher, H., 1996. Colloid-facilitated transport of strongly sorbing contaminants in natural porous media: a laboratory column study. Environ. Sci. Technol. 30, 3118–3123.

Huber, N., Baumann, T., Niessner, R., 2000. Assessment of colloid filtration in natural porous media by filtration theory. Environ. Sci. Technol. 34, 3774–3779.

Kaplan, D.I., Bertsch, P.M., Adriano, D.C., Miller, W.P., 1993. Soil-borne mobile colloids as influenced by water flow and organic carbon. Environ. Sci. Technol. 27, 1193–1200.

Klute, A., Dirksen, C., 1986. Hydraulic conductivity and diffusivity: laboratory methods. In: Klute, A. (Ed.), Methods of Soil Analysis-Part I. ASA and SSSA, Madison, WI, pp. 687–734.

Ko, C.H., Bhattacharjee, S., Elimelech, M., 2000. Coupled influence of colloidal and hydrodynamic interactions on the RSA dynamic blocking function for particle deposition onto packed spherical collectors. J. Colloid Interf. Sci. 229, 554–567.

Kralchevsky, P.A., Denkov, N.D., 2001. Capillary forces and structuring in layers of colloid particles. Curr. Opin. Colloid Interf. Sci. 6, 383–401.

Kralchevsky, P.A., Nagayama, K., 2000. Capillary interactions between particles bound to interfaces, liquid films and biomembranes. Adv. Colloid Interf. Sci. 85, 145–192.

Kralchevsky, P.A., Paunov, V.N., Ivanov, I.B., Nagayama, K., 1992. Capillary meniscus interaction between colloidal particles attached to a liquid–fluid interface. J. Colloid Interf. Sci. 151, 79–94.

Kretzschmar, R., Barmettler, K., Grolimund, D., Yan, Y.D., Borkovec, M., Sticher, H., 1997. Experimental determination of colloid deposition rates and collision efficiencies in natural porous media. Water Resour. Res. 33, 1129–1137.

Kretzschmar, R., Borkovec, M., Grolimund, D., Elimelech, M., 1999. Mobile subsurface colloids and their role in contaminant transport. Adv. Agron. 66, 121–193.

Lazouskaya, V., Jin, Y., Or, D., 2006. Interfacial interactions and colloid retention under steady flows in a capillary channel. J. Interf. Colloid Sci. 303, 171–184.

Lenhart, J.J., Saiers, J.E., 2002. Transport of silica colloids through unsaturated porous media: experimental results and model comparisons. Environ. Sci. Technol. 36, 769–777.

Litton, G.M., Olson, T.M., 1996. Particle size effects on colloid deposition kinetics: evidence of secondary minimum deposition. Colloid Surf. A 107, 273–283.

McCarthy, J.F., McKay, L.D., 2004. Colloid transport in the subsurface. past, present, and future challenges. Vadose Zone J. 3, 326–337.

McCarthy, J.F., Zachara, J.M., 1989. Subsurface transport of contaminants-mobile colloids in the subsurface environment may alter the transport of contaminants. Environ. Sci. Technol. 23, 496–502.

O'Melia, C.R., 1990. Kinetics of colloidal chemical processes in aquatic systems. In: Stumm, W. (Ed.), Aquatic Chemical Kinetics: Reaction rates of processes in natural water. Wiley-Interscience, New York, pp. 447–474.

Oostrom, M., Dane, J.H., Lenhard, R.J., 2002. Fluid contents. In: Dane, J.H., Topp, G.C. (Eds.), Methods of Soil Analysis-Part 4 Physical Methods. ASA and SSSA, Madison, WI, pp. 1539–1563.

Ruckenstein, E., Prieve, D.C., 1976. Adsorption and desorption of particles and their chromatographic separation. AICHE J. 22, 276–283.

Ryan, J.N., Gschwend, P.M., 1994. Effects of ionic strength and flow rate on colloid release: relating kinetics to intersurface potential energy. J. Colloid Interf. Sci. 164, 21–34.

Saiers, J.M., Lenhart, J.J., 2003a. Colloid mobilization and transport within unsaturated porous media under transient-flow conditions. Water Resour. Res. 39, 1019. doi:10.1029/2002WR001370.

Saiers, J.E., Lenhart, J.J., 2003b. Ionic-strength effects on colloid transport and interfacial reactions in partially saturated porous media. Water Resour. Res. 39, 1256. doi:10.1029/2002WR001887.

Saiers, J.M., Hornberger, G.M., Gower, D.B., Herman, J.S., 2003. The role of moving air–water interfaces in colloid mobilization within the vadose zone. Geophys. Res. Lett. 30, 2083. doi:10.1029/2003GL018418.

Shang, J., Flury, M., Chen, G., Zhuang, J., 2008. Impact of flow rate, water content, and capillary forces on in situ colloid mobilization during infiltration in unsaturated sediments. Water Resour. Res. 44, W06411. doi:10.1029/2007WR006516.

Simons, D.B., Sentürk, F., 1992. Sediment Transport and Technology: Water and Sediment Dynamics. Water Resources Publication. p. 77.

Song, L.F., Elimelech, M., 1993. Dynamics of colloid deposition in porous media: Modeling the role of retained particles. Colloid Surf. A 73, 49–63.

Steenhuis, T.S., McCarthy, J.F., Crist, J.T., Zevi, Y., Baveye, P.C., Throop, J.A., Fehrman, R.L., Dathe, A., Richards, B.K., 2005. Reply to ''comments on 'pore-scale visualization of colloid transport and retention in partly saturated porous media'". Vadose Zone J. 4, 957–958.

Tien, C., Payatakes, A.C., 1979. Advances in deep-bed filtration. AIChE J. 25, 737–759.

Torkzaban, S., Bradford, S.A., van Genuchten, M.T., Walker, S.L., 2008. Colloid transport in unsaturated porous media: the role of water content and ionic strength on particle straining. J. Contam. Hydrol. 96, 113–127.

Tyner, J.S., Brown, G.O., 2004. Improvements to estimating unsaturated soil hydraulic properties from horizontal infiltration. Soil Sci. Soc. Am. J. 68, 1–6.

van Genuchten, M.T., 1980. A closed form equation for predicting the hydraulic conductivity of unsaturated soils. Soil Sci. Soc. Am. J. 44, 892–898.

Wan, J., Tokunaga, T., 1997. Film straining of colloids in unsaturated porous media: conceptual model and experimental testing. Environ. Sci. Technol. 31, 2413–2420.

Wan, J., Tokunaga, T., 2002. Partitioning of clay colloids at air-water interfaces. J. Colloid Interf. Sci. 247, 54–61.

Wan, J., Tokunaga, T., 2005. Comments on ''pore-scale visualization of colloid transport and retention in partly saturated porous media". Vadose Zone J. 4, 954–956.

Worrall, F., Parker, A., Rae, J.E., Johnson, A.C., 1999. A study of suspended and colloidal matter in the leachate from lysimeters and its role in pesticide transport. J. Environ. Qual. 28, 595–604.

Zevi, Y., Dathe, A., McCarthy, J.F., Richards, B.K., Steenhuis, T.S., 2005. Distribution of colloid particles onto interfaces in partly saturated sand. Environ. Sci. Technol. 39, 7055–7064.

Zhuang, J., Flury, M., Jin, Y., 2003. Colloid-facilitated cesium transport through water-saturated Hanford sediments and Ottawa sand. Environ. Sci. Technol. 37, 4905–4911.

Zhuang, J., Jin, Y., Flury, M., 2004. Comparison of Hanford colloid and kaolinite transport in porous media. Vadose Zone J. 3 (2), 395–402.

Zhuang, J., Qi, J., Jin, Y., 2005. Retention and transport of amphiphilic colloids under unsaturated flow conditions: effect of particle size and surface properties. Environ. Sci. Technol. 39, 7853–7859.

Zhuang, J., McCarthy, J.F., Tyner, J.S., Perfect, E., Flury, M., 2007. In situ colloid mobilization in Hanford sediments under transient unsaturated flow conditions: effect of irrigation pattern. Environ. Sci. Technol. 41, 3199–3204.